Comparison of Three Radiative Formulations for Interactions in Three-Dimensional Boundary Layers

G. N. Kumar*
Tuskegee Institute, Tuskegee, Alabama
and
R. I. Vachon†
Vachon, Nix, & Associates, Atlanta, Georgia

This paper presents a comparison of analyses using three radiative interaction formulations to evaluate the effects of an external source of thermal radiation on the three-dimensional hypersonic turbulent boundary layer on a sharp cone at an angle of attack. The three radiative formulations considered are: 1) optically thin limit approximation, 2) optically thick limit approximation for the optical thickness of the medium, and 3) "band" approximation for the wavelength-dependent properties of the medium. For each of these formulations, interactions between radiation from an external source and the hypersonic boundary layer on a cone at an angle of attack are determined by solving numerically the three-dimensional compressible turbulent boundary-layer equations together with the energy equation modified to include thermal radiation. Turbulence is accounted for by making use of Prandtl's mixing length hypothesis with van Driest's modification for the wall region. Local nonsimilarity in the axial direction has been used to facilitate the numerical solution. Velocity and temperature fields, heat-transfer rates, and axial and normal aerodynamic coefficients have been compared for the three formulations at different Reynolds and Mach numbers. Even though the band approximation model is in general the most accurate of the three formulations considered, the results indicate that because of the extensive CPU time needed for this model it is not recommended for application to the problem under study.

Nomenclature

A_c = surface area of the cone
B = wavelength dependent Planck function, $B_\lambda(t) = e_{\lambda b}(t)/\pi$
C_A = axial aerodynamic coefficient, $= FAT/(\frac{1}{2}\rho_\infty u_\infty^2 A_c)$
C_N = normal aerodynamic coefficient, $= FNT/(\frac{1}{2}\rho_\infty u_\infty^2 A_c)$
C_p = specific heat at constant pressure
E_n = nth-order exponential integral; $E_n(t) = \int_0^1 m^{n-2} e^{-t/m}\,dm$
e_b = blackbody emissive power
FAT, FNT = total force on the cone in the axial and normal directions, respectively
Fbb = function given by Eq. (17)
Fbb_w = fraction of radiative heat flux emitted by the cone surface which is in the wavelength interval 0 to λ_c
Fbb_∞ = fraction of the radiative heat flux from the external source incident at the edge of the boundary layer which is in the wavelength interval 0 to λ_c
h = Planck's constant
$h', \bar{h}$ = fluctuating and mean static enthalpy, respectively
I_λ = intensity of radiation at wavelength λ
k' = Boltzmann constant
$\bar{k}, \bar{k}_t$ = laminar and eddy thermal conductivity, respectively
ℓ = mixing length for three-dimensional flow
L = axial length of the body
M_∞ = freestream Mach number
Nu = Nusselt number
P = nondimensional pressure, $= \bar{p}/\rho_\infty u_\infty^2$
P_∞ = freestream static pressure
$\bar{p}$ = local static pressure
Q_{conv} = convective heat transfer to wall
Q_{total} = total (convective plus radiative) heat transfer to wall
q = heat flux
q_r = radiant heat flux
q_s = radiation source intensity
q_w^r = radiative heat flux emitted by the surface of the cone which is assumed black
q_∞^r = radiative heat flux from the external source incident at the edge of the boundary layer
q^* = dimensionless heat-transfer rate nondimensionalized by $q^* = q/\rho_\infty u_\infty^3$
R = gas constant
r = radial coordinate defined in Fig. 1
r^* = nondimensional radial coordinate defined by $r^* = r/L$
Re_∞ = freestream Reynolds number
St_∞ = local Stanton number based on freestream conditions, $(q_w)/[\rho_\infty u_\infty C_p(T_0 - T_w)]$
T = nondimensional temperature, $= \dfrac{\bar{t}}{u_\infty^2/R}$
$\bar{t}$ = mean static temperature
u', v', w' = fluctuating streamwise, normal, and cross-flow velocity components, respectively
$\bar{u}, \bar{v}, \bar{w}$ = mean, normal, and cross-flow streamwise velocity components, respectively
u_∞ = freestream velocity
X, Y = nondimensional axial and normal coordinates, $X = x/L$, $Y = y/L$
x, y = axial and normal coordinates, respectively, defined in Fig. 1

Presented as Paper 82-0911 at the AIAA/ASME Third Joint Thermophysics, Fluids, Plasma, and Heat Transfer Conference, St. Louis, Mo., June 7-11, 1982; submitted May 5, 1983; revision received Nov. 28, 1983.

*Professor, Mechanical Engineering Department. Member AIAA.
†President. Member AIAA.

α = angle of attack
δ_v = sharp cone semivertex angle
ϵ = eddy viscosity for three-dimensional flow
ζ = similarity variable in the circumferential direction, $=\phi$
η = nondimensional normal coordinate, $=\sqrt{3/2P_e X}\int_0^Y \rho^* dY$
θ = nondimensional temperature T/T_e
λ = wavelength
κ = radiation absorption coefficient
κ_1, κ_2 = two-step model absorption coefficients, Eqs. (15) and (16)
μ = laminar viscosity
ξ = transformed axial coordinate, $=\int_0^X r^{*2} dX$
$\rho_0, \rho', \bar{\rho}$ = standard, fluctuating, and mean mass density, respectively
ρ^* = dimensionless density, nondimensionalized by $\rho^* = \bar{\rho}/\rho_\infty$
σ = Stefan-Boltzmann constant
τ = shear stress or optical thickness
$\tau_{0\lambda}$ = monochromatic optical thickness at the edge of the boundary layer
ϕ = circumferential coordiante defined in Fig. 1

Superscripts

$(\ )'$ = fluctuating component
$(\ \bar{}\ )$ = time average
r = due to radiation

Subscripts

b = blackbody
e = outer edge of boundary layer
i,j = used for summation purposes
w = wall
x,y = x and y directions, respectively
$1,2,\ldots$ = properties in two-step model absorption coefficient; also, order of exponential intergrals
0 = stagnation or total
∞ = freestream
λ = wavelength-dependent property
ν = frequency-dependent property
ϕ = circumferential direction

Introduction

THE problem of computing the effects of an external source of thermal radiation on the hypersonic flow past a sharp cone is one of importance in the analysis of the effect of a blast environment on the dynamics of hypersonic interceptor vehicles. The blast creates a thermally radiating fireball and this radiation interacts with the freestream, the vehicle boundary layer, and the shock layer. The overall problem is a complex one which may involve blast-shock interactions and thus needs to be divided into several subproblems. These subproblems need to be integrated to obtain the total effect. The present study encompasses the subproblem of evaluating the effects of an external source of thermal radiation on the boundary layer over the cone. The changes in the temperature and velocity fields in the boundary layer on the cone due to the external source and flight conditions and the concomitant changes in aerodynamic and force components are determined. This type of analysis forms the basis for determining the effect of an external source of thermal radiation on the hypersonic vehicle trajectory.

Even for simple flow situations, the mathematical complexity involved in the solution of conservation equations, when radiative interaction has been included, has led most investigators to consider the limiting cases of optical thickness, namely, the optically thin limit and optically thick limit approximations for the medium. In the present paper, for the problem under study, the above two limiting cases for participation by the medium are compared with the "band approximation" formulation where the radiative properties of the medium are approximated by breaking the wavelength spectrum into "bands" so that within each band the radiative properties of the medium (mainly the absorption coefficient) are constant with respect to wavelength and are functions of the local temperature and density only. The optically thin formulation as applicable to the present study has been discussed in detail in an earlier work by the authors.[1] Recently, the authors have presented a paper on the band approximation model.[2]

This simplified problem studied is depicted in Fig. 1. The external source of thermal radiation has been assumed to be a sphere of a given radius and known surface temperature at a given instant of time. The orientation of the cone with respect to the sphere is such that the axis of the cone is normal to a radial line from the center of the sphere. The cone surface has been assumed black and the external radiation incident at the edge of the boundary layer has been assumed diffuse. The thermal radiation reaching the edge of the boundary layer, in general, will be asymmetric as shown in Fig. 1. The radiation intensity incident at an elemental area at the edge of the boundary layer for a given orientation of the cone with respect to the radiation source was determined by a computer code developed by Dummer and Breckenridge,[3] and modified by Johnson,[4] to suit the present analysis. For each of the above formulations, the governing conservation equations are then transformed to reduce the number of independent variables. The coupled nonlinear transformed equations then are solved numerically to yield temperature and velocity fields, heat-transfer rates, as well as axial and normal aerodynamic coefficients for different Reynolds and Mach numbers for a given strength of the external source of thermal radiation.

Governing Equations

The coordinate directions used for the geometry under consideration are defined in Fig. 1. Heat is exchanged between the surface, the fluid in the boundary layer, and the surrounding fluid by convection and radiation, while heat is transferred to the surface of the cone and the fluid in the boundary layer from external source by radiation. It should be noted, however, that in the present simplified model of the overall problem, the emission or absorption of radiation across the shock layer has not been included. Thus the thermal radiation from the source is assumed to reach the edge of the boundary layer practically unattenuated. For a

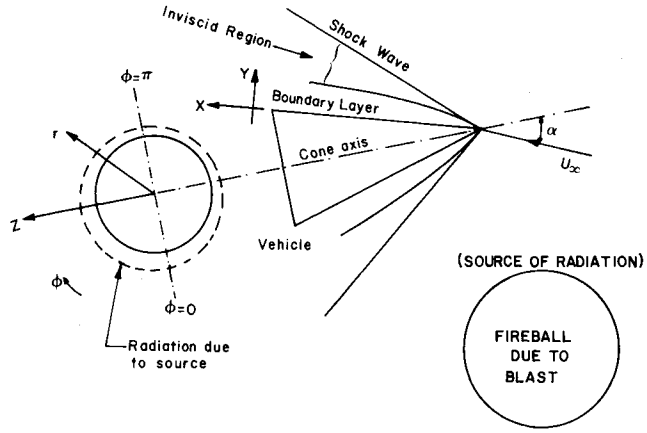

Fig. 1 Hypersonic vehicle near an external source of thermal radiation.

more accurate analysis of the overall problem, output from the shock analysis which includes radiative interaction should be used as input to the present boundary-layer analysis technique to effect a solution to the entire flowfield.

The governing conservation equations applicable to the problem under study are given by[1,2,5]:

Continuity:

$$\frac{\partial}{\partial x}(\bar{\rho}\bar{u}\bar{r}) + \frac{\partial}{\partial \phi}(\bar{\rho}\bar{w}) + \frac{\partial}{\partial y}[r(\bar{\rho}\bar{v} + \overline{\rho' v'})] = 0 \tag{1}$$

Streamwise (x) momentum:

$$\bar{\rho}\bar{u}\frac{\partial \bar{u}}{\partial x} + \frac{\bar{\rho}\bar{w}}{r}\frac{\partial \bar{u}}{\partial \phi} + (\bar{\rho}\bar{v} + \overline{\rho' v'})\frac{\partial \bar{u}}{\partial y} - \frac{\bar{\rho}\bar{w}^2}{r}\frac{\partial r}{\partial x} = -\frac{\partial \bar{p}}{\partial x} + \frac{\partial}{\partial y}\left[\mu\frac{\partial \bar{u}}{\partial y} - \bar{\rho}\overline{u' v'}\right] \tag{2}$$

Circumferential (ϕ) momentum:

$$\bar{\rho}\bar{u}\frac{\partial \bar{w}}{\partial x} + \frac{\bar{\rho}\bar{w}}{r}\frac{\partial \bar{w}}{\partial \phi} + (\bar{\rho}\bar{v} + \overline{\rho' v'})\frac{\partial \bar{w}}{\partial y} + \frac{\bar{\rho}\bar{u}\bar{w}}{r}\frac{\partial r}{\partial x} = -\frac{1}{r}\frac{\partial \bar{p}}{\partial \phi} + \frac{\partial}{\partial y}\left[\mu\frac{\partial \bar{w}}{\partial y} - \bar{\rho}\overline{v' w'}\right] \tag{3}$$

Normal (y) momentum:

$$\frac{\partial \bar{p}}{\partial y} = 0 \tag{4}$$

Energy:

$$\bar{\rho}\bar{u}\frac{\partial \bar{h}}{\partial x} + \frac{\bar{\rho}\bar{w}}{r}\frac{\partial \bar{h}}{\partial \phi} + (\bar{\rho}\bar{v} + \overline{\rho' v'})\frac{\partial \bar{h}}{\partial y} = \bar{u}\frac{\partial \bar{p}}{\partial x} + \frac{\bar{w}}{r}\frac{\partial \bar{p}}{\partial \phi} + \mu\left[\left(\frac{\partial \bar{u}}{\partial y}\right)^2 + \left(\frac{\partial \bar{w}}{\partial y}\right)^2\right] - \bar{\rho}\overline{u' v'}\frac{\partial \bar{u}}{\partial y} - \bar{\rho}\overline{v' w'}\frac{\partial \bar{w}}{\partial y} + \frac{\partial}{\partial y}\left[\frac{\mu}{Pr}\frac{\partial \bar{h}}{\partial y} - \bar{\rho}\overline{v' h'}\right] - \nabla \cdot q^r \tag{5}$$

where q^r is the radiation interaction with the boundary layer due to both the local radiation and the external sources.

Reynolds' stresses then can be written in terms of eddy viscosity as

$$-\bar{\rho}\overline{u' v'} = \epsilon_x \frac{\partial \bar{u}}{\partial y}, \qquad -\bar{\rho}\overline{v' w'} = \epsilon_y \frac{\partial w}{\partial y} \tag{6}$$

Similarly, the turbulent heat flux is expressed by

$$-\bar{\rho}\overline{v' h'} = \frac{\bar{k}_t}{C_p}\frac{\partial \bar{h}}{\partial y} \tag{7}$$

An order of magnitude analysis of the radiative flux terms in the energy equation was made.[6,7] This indicated that the radiation contribution in both the streamwise and circumferential directions can be neglected in comparison with the convection in these directions.

Radiant Energy Transfer

An expression for $\nabla \cdot q^r$ needed in the energy equation for the three radiation formulations considered is given below for the flow model shown in Fig. 2. Since radiant energy is propagated at the speed of light, it is necessary to consider fluid motion only if the vehicle speed would approach the speed of light. The fluid is assumed to be nonscattering. The fluid is also assumed to be gray for the optically thin and optically thick limit formulations. In the present analysis, it has been assumed that the cone surface is black and the external radiative flux incident at the edge of the boundary layer is diffuse. For the flow model of Fig. 2, based on the development by Sparrow and Cess,[8] the following expressions for the total net radiative flux q^r and the divergence of the radiative flux $\partial q^r/\partial y$ are obtained:

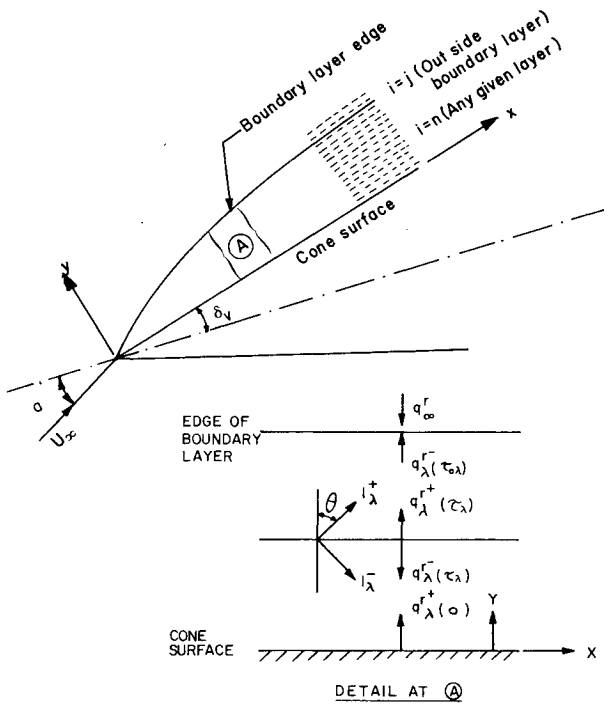

Fig. 2 Cone surface with optical coordinates.

$$q^r = 2\int_0^\infty \left\{\pi\int_0^{\tau_\lambda} B_\lambda(t)E_2(\tau_\lambda - t)\,dt + \pi I_\lambda^+(0)E_3(\tau_\lambda) - \pi\int_{\tau_\lambda}^{\tau_{0\lambda}} B_\lambda(t)E_2(t-\tau_\lambda)\,dt - \pi I_\lambda^-(\tau_{0\lambda})E_3(\tau_{0\lambda}-\tau_\lambda)\right\}d\lambda \tag{8}$$

and

$$-\frac{\partial q^r}{\partial y} = -\int_0^\infty \kappa_\lambda \frac{\partial q_\lambda^r}{\partial \tau_\lambda}\,d\lambda = 2\int_0^\infty \kappa_\lambda \left\{\pi\int_0^{\tau_{0\lambda}} B_\lambda(t)E_1(|t-\tau_\lambda|)\,dt - 2\pi B_\lambda(\tau_\lambda) + \pi I_\lambda^+(0)E_2(\tau_\lambda) + \pi I_\lambda^-(\tau_{0\lambda})E_2(\tau_{0\lambda}-\tau_\lambda)\right\}d\lambda \tag{9}$$

where the subscript 0 refers to the edge of the boundary layer. The expression for $\partial q^r/\partial y$ given by Eq. (9) will now be simplified for the three radiative interaction models considered, namely: 1) the optically thin medium approximation, 2) the optically thick medium approximation, and 3) the band approximation formulation.

Optically Thin Medium Approximation

The optically thin medium approximation, as applicable to the flow model under consideration, has been discussed in detail in an earlier paper by the authors[1] and will not be

repeated here. For this model, Eq. (9) simplifies to

$$-\frac{dq^r}{dy}=2\kappa[\sigma t_w^4+q^r_\infty-2\sigma t^4(y)] \tag{10}$$

where q^r_∞ is the radiant heat flux from the external source incident at the edge of the boundary layer, and the absorption coefficient $\kappa(t)$ is given by[9]

$$\kappa(t)=71.29\left(\frac{\rho_\infty}{\rho_0}\right)\left(\frac{t}{10^4}\right)^5 \text{cm}^{-1} \tag{11}$$

Optically Thick Medium Approximation

For an optically thick medium approximation, the radiant energy transfer depends only on conditions in the immediate vicinity of the position being considered and is described only in terms of the gradient of the conditions at that position. The fluid is again assumed to be nonscattering and gray. For the problem under study, for the optically thick medium, Eq. (9) then simplifies to[8]

$$-\frac{\partial q^r}{\partial y}=\frac{\partial}{\partial y}\left[\frac{4\sigma}{3\kappa_R}\frac{\partial t^4}{\partial y}\right] \tag{12}$$

and the variation of the Rosseland mean absorption coefficient κ_R with temperature and pressure is given by[10]

$$\rho\kappa_R=4.5\times10^{-7}P^{-1.31}[\exp 5.18\times10^{-4}t-7.13\times10^{-7}t^2] \tag{13}$$

where $\rho\kappa_R$ is in cm^{-1}, P is in atmospheres, and t is in degrees Kelvin.

Two-Band Approximation Formulation

This formulation has been discussed in an earlier paper by the authors.[2] From Eq. (9) it can be seen that, for the divergence of radiative flux term, there are actually two integrals to be evaluated at every point in the flowfield. The two integrals are

Wavelength integral $\int_0^\infty f(\lambda)\,d\lambda$

Spatial integral $\int_0^{\tau_{0\lambda}} g(t)\,dt$

Table 1 Constant for the O_2 continuum absorption band absorption coefficient, Eq. (15)

T, K (Range)	Up to 3,000	3,000-4,000	4,000-6,000	6,000-7,000	7,000-8,000	8,000-11,000
a	12.5	2.13	0.0263	0.0265	0.061	0.1717
b	1.0	1.16	1.6	1.46	1.41	1.6
c	−0.65	−2.1	−7.1	−6.67	−1.34	−1.34

Table 2 Constants for the long wavelength band absorption coefficient, Eq. (16)

T, K (Range)	Up to 4,000	4,000-6,000	6,000-8,000	8,000-11,000
a	0.013	0.061	0.0425	0.034
b	1.1	1.4	1.4	1.37
c	3.0	4.6	4.0	2.9

In the band approximation formulation, emission and absorption will be accounted for in the flowfield using the general equation containing spatial integral terms for one-dimensional radiation transport. However, as far as integration with respect to wavelength is concerned, in order to evaluate the wavelength integral, which is independent of the spatial integral, the wavelength spectrum is broken into "two bands" such that

$$\begin{aligned}\kappa(\lambda,\rho,t)&=\kappa_1(\rho,t): && 0\le\lambda\le\lambda_c\\ &=\kappa_2(\rho,t): && \lambda_c\le\lambda\le\infty\end{aligned} \tag{14}$$

The absorption coefficient is now constant with the wavelength for each band and is a function of only the local temperature and density.

The "band approximation" may be extended to as many bands as desired. However, it has been shown by Chin,[11] Anderson,[12] and Lilly[13] that a good approximation of the absorption coefficient can be made with the two-band approximation model given below.

For the photon energy range of 7.1 to ∞ (wavelength range 0-1730 Å), the following expression was developed for the absorption coefficient κ_1,[13]

$$\kappa_1=a\left(\frac{\rho}{\rho_0}\right)^b\left(\frac{t}{10^4}\right)^c \tag{15}$$

where a, b, and c are given in Table 1.

In a similar manner, average absorption coefficients for photon energies up to 7 eV (wavelength interval 1730 Å → ∞) are given by[13]

$$\kappa_2=\frac{a}{(1-Fbb)}\left(\frac{\rho}{\rho_0}\right)^b\left(\frac{t}{10^4}\right)^c \tag{16}$$

with the values of a, b, and c given in Table 2. Fbb is the fraction of blackbody radiation up to wavelength λ_c and is given by[11]

$$Fbb(x)=\frac{15}{4}\sum_{m=1}^{\infty}\frac{e^{-mx}}{m^4}\{[(mx+3)mx+6]mx+6\} \tag{17}$$

where $x=h\nu_c/k't$.

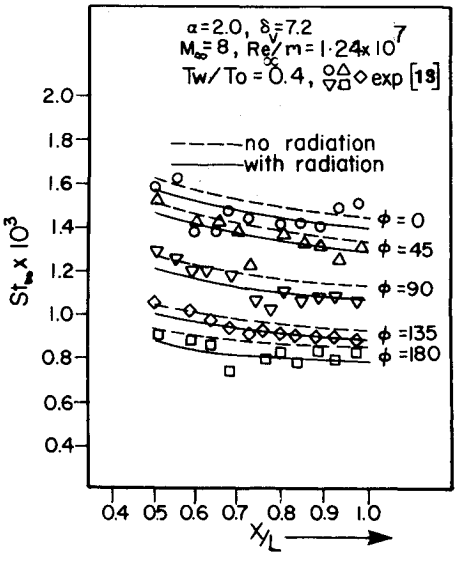

Fig. 3 Comparison of Stanton number with experimental values.

For a given axial position, at any distance y from the surface, the integration of Eqs. (8) and (9) with respect to y (the spatial integral) is done by dividing the boundary-layer thickness into a finite number (j) of layers as shown in Fig. 2 and writing the integral as summation over the j layers. The expressions for the net radiative flux and the divergence of the radiative flux at any location n in the boundary layer can be written as[13,2]:

$$q_n^r = 2\sigma \sum_{i=1}^{n} t_i^4 [Fbb_i E_2(\tau_{1n}-\tau_{1i})\Delta\tau_{1i} + (1-Fbb_i)E_2(\tau_{2n}-\tau_{2i})\Delta\tau_{2i}] + 2[Fbb_w \sigma t_w^4 E_3(\tau_{1n}) + (1-Fbb_w)\sigma t_w^4 E_3(\tau_{2n})] - 2\sigma \sum_{i=n}^{j} t_i^4 [Fbb_i E_2(\tau_{1i}-\tau_{1n}) \times \Delta\tau_{1i} + (1-Fbb_i)E_2(\tau_{2i}-\tau_{2n})\Delta\tau_{2i}] - 2[Fbb_\infty q_\infty^r E_3 \times (\tau_{1j}-\tau_{1n}) + (1-Fbb_\infty) q_\infty^r E_3(\tau_{2j}-\tau_{2n})] \quad (18)$$

and

$$-\frac{\partial q_n^r}{\partial y} = 2\sigma \sum_{i=1}^{j} t_i^4 [Fbb_i \kappa_{1i} E_1(|\tau_{1n}-\tau_{1i}|)\Delta\tau_{1i} + (1-Fbb_i)\kappa_{2i}E_1(|\tau_{2n}-\tau_{2i}|)\Delta\tau_{2i}] - 4\sigma t_n^4 \kappa_{1n} Fbb_n - 4\sigma t_n^4 \kappa_{2n}(1-Fbb_n) + q_w^r [Fbb_w \kappa_{11} E_2(\tau_{1n}) + (1-Fbb_w)\kappa_{21}E_2(\tau_{2n})] + q_\infty^r [Fbb_\infty \kappa_{1j} E_2(\tau_{1j}-\tau_{1n}) + (1-Fbb_\infty)\kappa_{2j}E_2(\tau_{2j}-\tau_{2n})] \quad (19)$$

with the exponential integrals E_1, E_2, and E_3 evaluated using the formulas suggested by Schwartz.[14]

The expression for the divergence of the radiative heat flux from Eq. (10), (12), or (19) must be added to the energy equation to include the effects of an external source of radiation for the three formulations considered.

The case $i=n$ in Eq. (19) needs to be handled a little differently since $E_1(t)\to\infty$ as $t\to 0$. For this case, using Eq. (18), q_j^r is evaluated for layers $j=n-3$ to $n+3$, and then by numerical differentiation divergence of the radiative flux term $(-\partial q_n^r/\partial y)$ is obtained.

Solution of the Boundary-Layer Equations

As already developed in the earlier papers by the authors,[1,2] Eqs. (1-5) can be put in nondimensional form using the similarity variables ξ, η, and ϕ.

The mixing length distribution needed for the solution of conservation equations is based on the development of Adams.[5] In consists of a two-layer inner-outer model using Prandtl's hypothesis and a modification of van Driest's analysis for the near-wall region.[15] The eddy viscosity in the transformed variables for the two regions is listed in Ref. 2 and will not be repeated here.

For solution of the transformed governing equations, boundary conditions must be specified at $\phi=0$ for $0\le y\le y_e$ and along the surfaces $y=0$ and $y=y_e$ for $0\le\phi\le 180$ deg. The conditions at $y=0$ are obtained from the "no-slip" requirement. The inviscid conditions at the outer edge of the boundary layer are obtained from Ref. 16. Advantage is taken of symmetry in the plane $\phi=0$ to generate a starting solution.

In the present study, since the governing equations become nonsimilar because of the dependence of the turbulent viscosity and the radiative heat flux on the streamwise coordinate "local nonsimilarity" was assumed, i.e., the equations were solved at fixed values of ξ. The justification for this local nonsimilarity method is given in Ref. 1. The numerical solution of the transformed governing equations in similarity variables ξ, η, and ϕ follows the method described by the authors in their earlier paper[1] and will not be detailed here.

Inviscid conditions at the outer edge of the boundary layer are determined based on the results of an inviscid analysis of a sharp cone at incidence by Jones.[17]

The CPU time required for running the computer code for a given set of Mach number, Reynolds number, and angles of attack on an IBM 370/158 computer was on the order of 50 min for the optically thick formulation, 100 min for the optically thin formulation, and 250 min for the band approximation formulation. A copy of the computer code for each of the formulations considered can be obtained from the authors.

Comparison with Experimental Results

Comparison of the Stanton numbers obtained from the present study with the experimental data of Martellucci and Neff,[18] as presented by Adams,[5] is made in Fig. 3. Since there was no external source of thermal radiation included in the above experiments (radiative interaction in the boundary layer was due only to the difference in temperature between the freestream and wall and was very small), the three radiation formulations gave the Stanton number values which were very close to each other and have been shown plotted as one curve in Fig. 3. It can be seen that the results of the present analysis, which include thermal radiation in the boundary layer, are in good agreement with the data. This comparison of the solution from the computer codes used in the present study with the experimental data provides confidence that the formulation and solution technique are producing results consistent with observation.

Results and Discussion

In the present study, since the CPU time needed for each run (especially for the band approximation formulation) is large, as mentioned above, the total number of runs that could be made for each of the three formulations had to be limited. A few of the main parameters were kept constant to minimize the computer time required and to obtain the precise effects of parameters, namely, Re_∞ and M_∞. All of the calculations were done for a source intensity of 1.459×10^8 W/m^2 at 610 m from the cone axis. The fireball (source) diameter was taken to be 610 m. The results shown are for a cone with a cone half-angle of 6 deg and a length of 2.6534 m. In this section, results from the three radiation formulations are compared with each other and with the corresponding case with no radiation. No specific parametric study with respect to nondimensional radiation parameters such as Boltzmann number and conduction to radiation parameter was made in the present work because of CPU time limitations.

Mean static temperature profiles in the boundary layer are compared in Fig. 4. This figure shows that, of the three formulations, the optically thick formulation gives the steepest slope near the wall. Since the local absorption of incident radiation for the optically thick case is high compared to the other two formulations, these absorptions give rise to higher local temperatures compared to the other two radiation formulations and the no-radiation case. Band approximation always gives values which are between those predicted by optically thin and optically thick formulations. Figure 4b shows that the temperature profiles at $M_\infty=16$ are different from those at $M_\infty=4$. At $M_\infty=16$, as shown in Fig. 4b, the temperature increases very rapidly close to the wall and then decreases gradually to the value at the edge of the thermal boundary layer. The temperature gradients close to the wall thus increase with Mach number. This is because viscous dissipation is more at high Mach numbers of the freestream compared to the low Mach numbers. Hence,

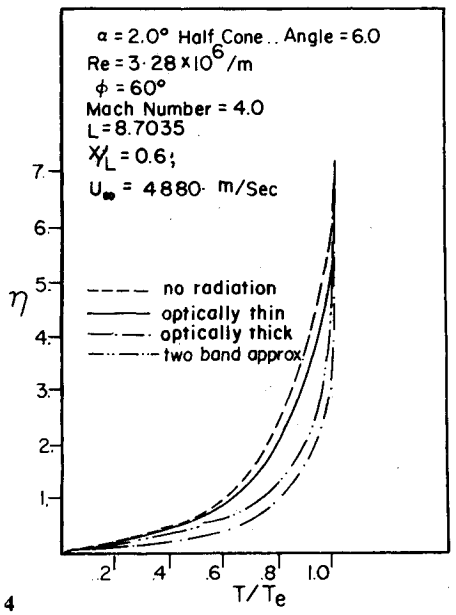

a) $M_\infty = 4$

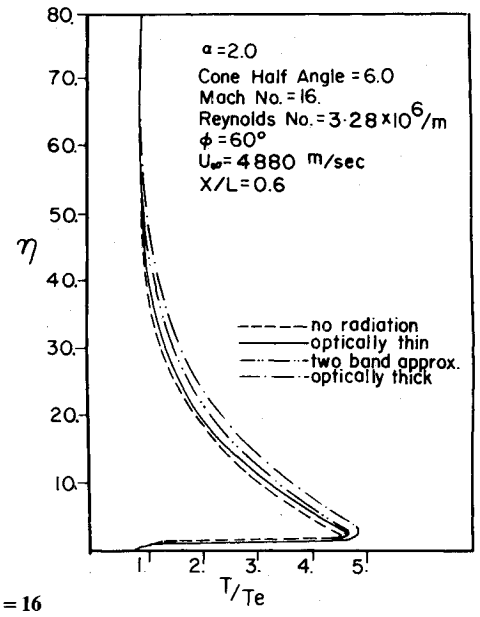

b) $M_\infty = 16$

Fig. 4 Effect of radiation on static temperature ratio.

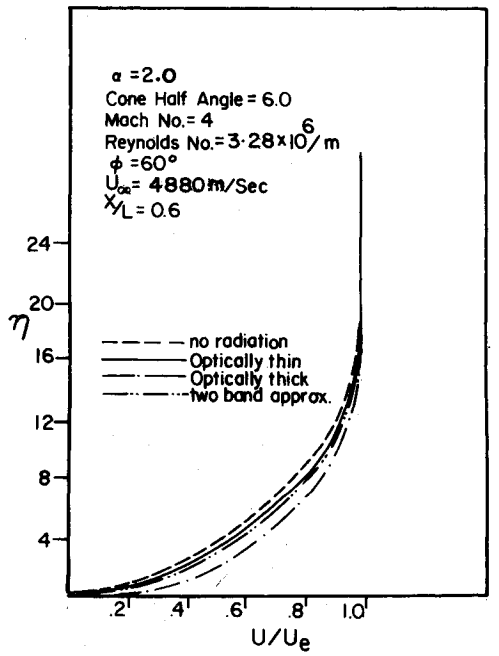

Fig. 5 Comparison of streamwise velocity profiles.

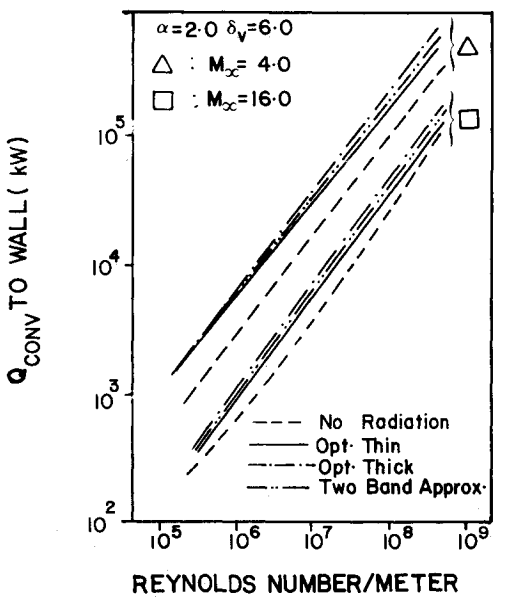

Fig. 6 Comparison of convective heat transfer to wall for different formulations.

because of increased dissipation effects, fluid temperature reaches a maximum value at some point in the boundary layer (close to the wall) and the heat actually will be transferred from that point, both toward the wall and toward the external source.

Streamwise velocity profiles are compared in Fig. 5. The velocity profile is similar in shape to the temperature profile of Fig. 4a. As before, of the three radiative formulations, the optically thick formulation has the maximum slope near the wall. This is because radiative interaction in the boundary layer, due to the optically thick formulation, causes greater changes in properties such as local density and viscosity compared to the other two formulations. At a given axial location, if the velocity profiles at different Mach numbers are compared (figures not shown due to space limitations), they show that gradients near the wall increase with Mach numbers and that the boundary-layer thickness is reduced as M_∞ is increased. Cross-flow velocity profiles also show the general trend of Fig. 5.

Convective heat transfer to the wall for the different formulations is compared in Fig. 6. As seen in this figure, the three radiative formulations give about the same value for the convective heat transfer to the wall, although the optically thick values are slightly more than the other two. The slightly larger values for the optically thick case are due to its larger temperature gradients at the wall compared to the other two formulations. For each formulation, the increase of convective heat transfer with Re_∞ is due to the decrease in boundary-layer thickness with increase in Re_∞ which results in steeper temperature and velocity gradients at the wall. However, the ratio of convective heat transfer to the wall with radiation to that without radiation remains practically constant with variation of Re_∞ for a given M_∞ (figure not shown due to space limitations). Figure 6 also shows the convective heat transfer to the wall decreased as the Mach number increased. This is due to the fact that in the present analysis, as M_∞ is increased at constant Re_∞, the freestream temperature is reduced (for the cases under consideration t_∞ at $M_\infty = 4$ is 3700 K and at $M_\infty = 16$ is 231.1 K).

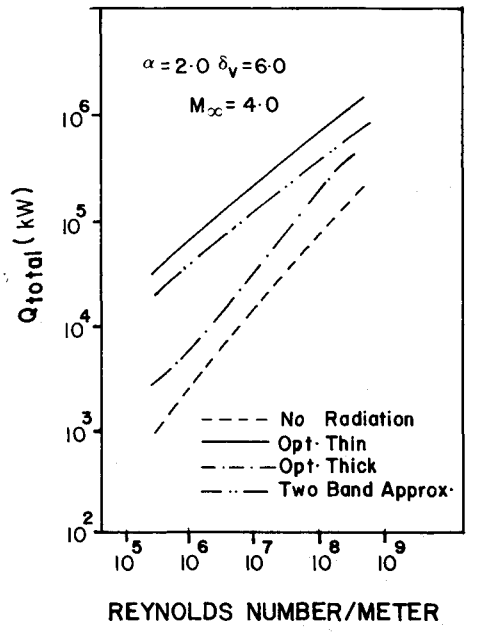

Fig. 7 Comparison of total heat transfer to wall for different formulations.

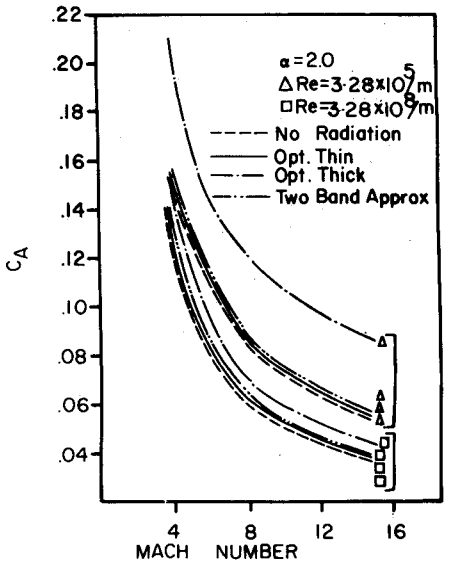

Fig. 8 Comparison of axial aerodynamic coefficients.

Table 3 Comparison of total heat transfer to the wall at constant Reynolds number ($\alpha = 2.0$, $U_\infty = 4877$ m/s, $Re_\infty/m = 3.281 \times 10^5$)

	Q_{total}, kW			
M_∞	No radiation, $\times 10^{-3}$	Optically thin, $\times 10^{-5}$	Band approximation, $\times 10^{-5}$	Optically thick, $\times 10^{-4}$
4	0.866	0.315	0.19	0.273
8	0.442	0.409	0.301	0.308
12	0.191	0.411	0.302	0.323
16	0.143	0.411	0.308	0.334

Table 4 Effect of angle of attack on axial aerodynamic coefficient ($M_\infty = 4.0$, $Re_\infty/m = 3.281 \times 10^5$, $U_\infty = 4877$ m/s)

	C_A			
α	No radiation	Optically thin	Band approximation	Optically thick
2	0.153	0.154	0.155	0.211
3	0.162	0.165	0.169	0.234
5	0.171	0.1755	0.180	0.283

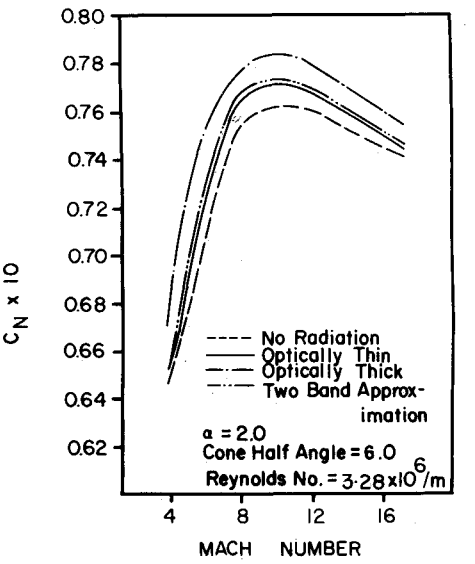

Fig. 9 Comparison of normal aerodynamic coefficients.

Figure 7 compares the total heat transfer to the wall (convective plus radiative) for different formulations. Since the convective heat transfer to the wall is approximately the same for the three radiation formulations, the difference in total heat transfer values among the three radiation formulations is due mainly to the radiative contribution at the wall. The radiative heat flux at the wall is more for the optically thin formulation compared to the other two because a larger fraction of incident radiative flux reaches the wall without being absorbed in the boundary layer. Similarly, for the optically thick formulation, most of the incident radiative flux is absorbed by the boundary layer and the fraction reaching the wall is small compared to the other two formulations. Figure 7 also shows that as Reynolds number is increased the radiative heat transfer to the wall (and also the total heat transfer to the wall) increases because as Re_∞ is increased, boundary-layer thickness reduces and the absorption in the boundary layer is reduced and more incident flux is transmitted directly to the wall.

Comparison of the effect of Mach number on the total heat transfer to the wall for the different formulations is made in Table 3. This table shows that even though convective heat transfer to the wall decreases as M_∞ increases for reasons explained previously, radiative heat transfer to the wall increases as M_∞ is increased. This is because as M_∞ is increased, for conditions imposed in this study, the absorption coefficient decreases and thus the radiative flux to the wall from the surrounding fluid decreases. But the fraction directly transmitted to the wall is increased and hence the total radiative flux at the wall increases as M_∞ increases. The absorption coefficient levels off at higher Mach numbers ($M_\infty > 8$). Hence, the increase in total heat transfer to the wall is very small at higher Mach numbers.

Figures 8 and 9 compare the axial and normal aerodynamic coefficients for the different formulations. These figures show that the increase in the value of these coefficients due to radiation is significant only for the optically thick formulation. This is because gradients at the wall (velocity and temperature) are higher for this formulation compared to the other two radiation formulations as explained previously.

The effect of angle of attack on the axial aerodynamic coefficient is shown in Table 4. This table shows that as the angle of attack is increased, the value of C_A increases by 10-30%, the maximum increase being for the optically thick case for the same reasons given above for Table 3. The effect of angle of attack on C_N is similar to that of C_A and is not reported here.

In summary, a solution technique developed by the authors[1] for the problem under study has been used to compare the effects of using three radiative interaction formulations. Comparison indicates that the total heat flux to the wall is increased by an order of magnitude due to the external source of radiation compared to the no-radiation case. It also shows that the increase in total heat transfer is maximum for the optically thin formulation. Comparison also indicates that as far as axial and normal aerodynamic coefficients are concerned, the influence of optically thin and band approximation models is negligible and only the optically thick formulation has some significant effect on these coefficients. The closeness of values from optically thin and band approximation formulations indicates that for the conditions under study, gas in the boundary layer behaves more like an optically thin gas. Even though the band approximation, in general, gives a more accurate representation of the radiative interaction effects compared to the other two formulations, because of the excessive CPU time needed for this formulation, it is not recommended for the problem under study. The optically thin formulation should give reasonably accurate results with moderate CPU times.

To obtain a more accurate solution of the overall problem described earlier, the analysis described above needs to be extended to include one or more of the following.

1) Couple the boundary-layer program with a radiating shock layer analysis.

2) Couple the present boundary-layer analysis with analysis of ablation from the surface.

3) Study the effect of varying the optical properties of the surface instead of assuming it is black or gray. The effect of wavelength dependency of external source of radiation can also be included.

4) Develop a two-dimensional radiation transport model.

Acknowledgments

The research reported herein was a result of sponsorship by the U. S. Army Ballistic Missile Defense Systems Command under Contract DASG60-75-0045. Appreciation is expressed to contract supervisor, James Papadopoulos.

References

[1] Kumar, G. N., Khader, M. S., and Vachon, R. I., "Interaction between Radiative and Convective Heat Transfer in the Hypersonic Boundary Layer on a Circular Cone at an Angle of Attack," AIAA Paper 80-1717, July 1980.

[2] Kumar, G. N. and Vachon, R. I., "Radiative and Convective Heat Transfer Interactions in the Three Dimensional Compressible Hypersonic Turbulent Boundary Layer on a Sharp Cone at an Angle of Attack," Paper presented at the 16th Southeastern Seminar on Thermal Sciences, Miami, Fla., April 1982; also, *Thermal Sciences 16*, Vol. 1, Hemisphere Publishing Corp., New York, 1983, pp. 419-422.

[3] Dummer, R. S. and Breckenridge Jr., W. T., "Radiation Configuration Factors Program," General Dynamics/Astronautics, San Diego, Calif., Rept. ERR-AN-224, Feb. 1963.

[4] Johnson, R. E., "Radiation Shape Factor and Loading Analysis on a Hypersonic Vehicle in the Vicinity of a Nuclear Blast," M.S. Thesis, Auburn University, Auburn, Ala., March 1977.

[5] Adams Jr., J. C., "Analysis of the Three-Dimensional Compressible Turbulent Boundary Layer on a Sharp Cone at Incidence in Supersonic and Hypersonic Flow," Arnold Engineering Development Center, Arnold Air Force Station, Tenn., AEDC-TR-72-66, June 1972; also, *International Journal of Heat and Mass Transfer*, Vol. 17, 1974, pp. 581-593.

[6] Kumar, G. N., "Interaction Between Radiative and Convective Heat Transfer in a Hypersonic Turbulent Boundary Layer on a Circular Cone at an Angle of Attack," Ph.D. Dissertation, Department of Mechanical Engineering, Auburn University, Auburn, Ala., Aug. 1978.

[7] Kumar, G. N., et al., "Part II, Blast Traversal Study: Effects of Asymmetrical Thermal and Dynamic Loads on Interceptor Performance," Final Report Contract DASG60-75-C-0045, Engineering Experiment Station, Auburn University, Auburn, Ala., Sept. 15, 1977.

[8] Sparrow, E. M. and Cess, R. D., *Radiation Heat Transfer*, Brooks/Cole Pub. Co., Belmont, Calif., 1966.

[9] Traugott, S. C., "Shock Structure in a Radiating, Heat Conducting, and Viscous Gas," *Physics of Fluids*, Vol. 8, 1965, pp. 834-849.

[10] Pai, S. I. and Tsao, C. K., "A Uniform Flow of Radiating Gas Over A Flat Plate," *Proceedings of the Third International Heat Transfer Conference*, American Institute of Chemical Engineers, Chicago, Ill., Vol. V, 1966, pp. 129-137.

[11] Chin, J. H., "Inviscid Radiating Flow Around Bodies Including the Effect of Energy Loss and Non-Grey Self-Absorption," Lockheed Missiles & Space Co., Sunnyvale, Calif., LMSC 668005, Oct. 1965.

[12] Anderson, Jr., J. D., "Stagnation Point Heat Transfer from a Viscous Non-Radiating Shock Layer," Naval Ordnance Laboratory, Corona, Calif., TR 67-189, Nov. 1967.

[13] Lilly, J. Q., "Analysis of Bow Shock Structure at a Stagnation Point Subjected to External Radiation," Ph.D. Dissertation, Mechanical Engineering Department, University of Alabama, Tuscaloosa, Ala., 1969; also, U.S. Army Missile Command, Redstone Arsenal, Ala., Rept. RS-TR-69-4, May 1969.

[14] Schwartz, J., "Radiation Effects in the Stagnation Region Boundary Layer," Aerophysics Laboratory, M.I.T., Cambridge, Mass., TR 119, Nov. 1965.

[15] van Driest, E. R., "On Turbulent Flow Near a Wall," *Journal of the Aeronautical Sciences*, Vol. 23, No. 11, 1956, pp. 1007-1011.

[16] Jones, D. J., "Numerical Solutions of the Flow Field for Conical Bodies in a Supersonic Stream," National Research Council of Canada, Ottawa, Canada, Aeronautical Rept. LR-507, July 1968; also, *C.A.S.I. Transactions*, Vol. 3, No. 1, March 1970, pp. 62-71.

[17] Jones, D. J., "Use of the Jones Computer Programme to Determine the Flow Field for Conical Flow Situations, Part I: The Circular Cone at Incidence," National Research Council of Canada, Ottawa, Canada, NAE LTR-HA-1, June 1969.

[18] Martellucci, A. and Neff, R. S., "The Influence of Asymmetric Transition on Re-entry Vehicle Motion," *Journal of Spacecraft and Rockets*, Vol. 8, May 1971, pp. 476-482; also, AIAA Paper 70-987.